Control over Self-Assembly of Diblock Copolymers on Hexagonal and Square Templates for High Area Density Circuit Boards

Jie Feng, Kevin A. Cavicchi, and Hendrik Heinz*

Department of Polymer Engineering, University of Akron, Akron, Ohio 44325, United States

ABSTRACT

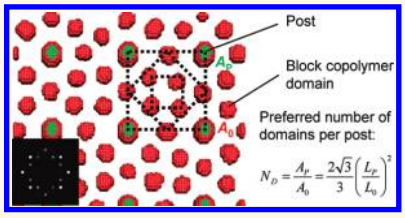

Self-assembled diblock copolymer melts on patterned substrates can induce a smaller characteristic domain spacing compared to predefined lithographic patterns and enable the manufacture of circuit boards with a high area density of computing and storage units. Monte Carlo simulation using coarse-grain models of polystyrene-*b*-polydimethylsiloxane shows that the generation of high-density hexagonal and square patterns is controlled by the ratio N_D of the surface area per post and the surface area per spherical domain of neat block copolymer. N_D represents the preferred number of block copolymer domains per post. Selected integer numbers support the formation of ordered structures on hexagonal (1, 3, 4, 7, 9) and square (1, 2, 5, 7) templates. On square templates, only smaller numbers of block copolymer domains per post support the formation of ordered arrays with significant stabilization energies relative to hexagonal morphology. Deviation from suitable integer numbers N_D increases the likelihood of transitional morphologies between square and hexagonal. Upon increasing the spacing of posts on the substrate, square arrays, nested square arrays, and disordered hexagonal morphologies with multiple coordination numbers were identified, accompanied by a decrease in stabilization energy. Control over the main design parameter N_D may allow an up to 7-fold increase in density of spherical block copolymer domains per surface area in comparison to the density of square posts and provide access to a wide range of high-density nanostructures to pattern electronic devices.

KEYWORDS: directed assembly · block copolymers · electronic devices · patterning · modeling and simulation · nanoscale circuitry · thin films

The demand for higher data storage capacity and miniature electronic devices drives the reduction of characteristic dimensions of storage media and circuit boards toward the nanometer scale. Compared to the resolution of conventional photolithographic techniques above 50 nm, characteristic dimensions below would accommodate a higher number of storage and computing units per area.[1−4] Block copolymers facilitate feature sizes of 5−50 nm of periodic lamellae, hexagonal cylinders, spheres, and gyroids[5] that can be exploited to pattern microelectronic substrates. However, self-assembled structures of neat block copolymers show defective long-range order, and perfect order up to centimeters can be achieved by use of topographical substrates and graphoepitaxy (templated overgrowth).[4,6,7] For example, hexagonal arrays of cylinders with center-to-center distances of 6.9 nm and perfect order over centimeters were assembled from poly(styrene)-*b*-poly(ethylene oxide) (PS-*b*-PEO) diblock copolymer films on corrugated substrates with a sawtooth pattern.[4] Hexagonal long-range order with a center-to-center spacing of 40 nm of spherical polydimethylsiloxane (PDMS) microdomains was also achieved using a poly(styrene)-*b*-poly(dimethylsiloxane) (PS-*b*-PDMS) diblock copolymer on a hydrogen silsesquioxane substrate with a hexagonal array of posts of ~200 nm spacing.[7]

Such hexagonal patterns of asymmetric diblock copolymers (DBCPs) with long-range order enable the manufacture of templates for magnetic storage media upon removal of the minor component.[4,7−9] However, square arrays of DBCP microdomains would be preferred over hexagonal arrays to manufacture circuit boards[3,10] and have been obtained using blends of DBCPs with specific hydrogen bonds,[3] square templates, and prepatterned surfaces.[11] For example, alignment of cylindrical microdomains of poly(styrene)-*b*-poly(methyl methacrylate) (PS-*b*-PMMA) into squares was possible on surfaces containing a square pattern of spots.[11] However, the area density of the

* Address correspondence to hendrik.heinz@uakron.edu.

Received for review March 15, 2011 and accepted October 29, 2011.

Published online October 30, 2011
10.1021/nn2035439

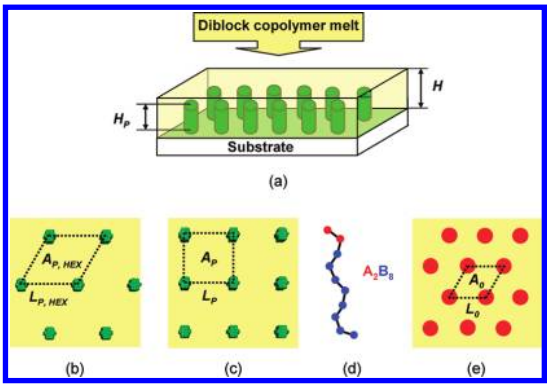

Figure 1. (a) Schematic representation of a substrate with a square array of posts of height H_P. The posts confine a diblock copolymer melt of thickness H. (b) Top view of the substrate in the simulation showing a hexagonal array of posts of spacing $L_{P,HEX}$ and the surface area per post $A_{P,HEX}$. (c) Top view of the substrate in the simulation showing a square array of posts of spacing L_P and the surface area per post A_P. (d) Model of a coarse-grain A_2B_8 block copolymer chain in which each segment represents several monomers. (e) In the absence of posts, the diblock copolymer melt forms a hexagonal array of domains A of spacing L_0 that encloses a surface area per domain A_0.

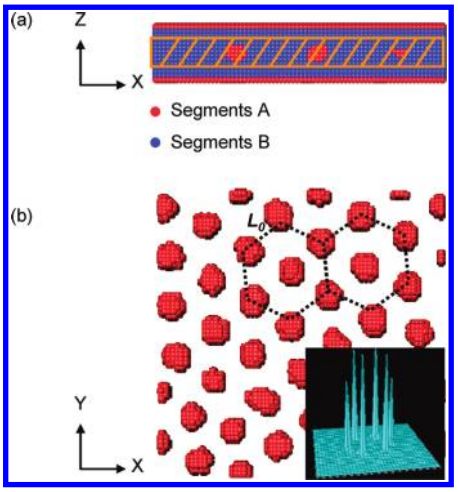

Figure 2. Computed average morphology of an A_2B_8 diblock copolymer film confined between two parallel flat substrates without posts. (a) The side view of a section in the *xz* plane shows the formation of a thin film of component A in contact with the substrate and of spherical domains of component A in the matrix of component B. (b) The top view of the highlighted cross-section in (a) shows the approximate hexagonal order of the spheres of component A and the equilibrium domain spacing L_0. The inset shows a Fourier transform of the position of domains A.

template could not be exceeded and notable fractions of defects such as semicylinders and loop cylinders prevent long-range order.[11,12]

Therefore, the preparation of high-density, well-defined square patterns remains a challenge. In this contribution, we have analyzed design parameters to increase hexagonal and square pattern densities using coarse-grain models and Monte Carlo simulation (Figure 1) and found that the ratio between the surface area per post and the surface area per neat block copolymer domain exerts critical influence on the order and stability of self-assembled patterns. Other factors, such as the composition and length of the polymer blocks, the thickness of the polymer film, and the geometry of posts, also play a role and will be briefly described.

We employed models of hexagonal and square patterns of vertical posts on flat substrates and simulated the assembly of melt-cast block copolymers (Figure 1a)[13−17] for a series of spacing $L_{P,\ HEX}$ and L_P between the confining posts (Figure 1b,c). Our model block copolymer A_2B_8 represents polystyrene-*b*-polydimethylsiloxane (PS-*b*-PDMS) of 140 repeat units and qualitatively similar block copolymers (Figure 1d). Each coarse-grain unit A and B embodies 14 monomer segments. The substrate (S), posts (P), monomer segments (A and B), and vacancies (V) are represented by coarse-grain lattice sites on a cubic lattice up to a dimension of 144 × 144 × 14 lattice sites. As in experiment,[7] substrate and post surfaces slightly prefer contact with component A over component B, which is represented by pairwise interaction parameters $\varepsilon_{SA} = \varepsilon_{PA} = 0$ and $\varepsilon_{SB} = \varepsilon_{PB} = 0.5k_BT$. Direct contact between segments A and B is subject to a small energy penalty $\varepsilon_{AB} = 0.5k_BT$, which reflects a positive interface tension. All other interactions involving components of the same type and vacancies are zero; $\varepsilon_{AA} = \varepsilon_{BB} = \varepsilon_{VV} = \varepsilon_{AV} = \varepsilon_{BV} = \varepsilon_{SV} = \varepsilon_{PV} = 0$ (see Methods section for a full description of models, computation, and analysis). This parameter choice corresponds to Flory−Huggins parameters $\chi_{AB} \approx 2.5$ and $\chi_{AB}N \approx 25$ using the approximate relation $\chi_{AB} \approx 5\varepsilon_{AB}/kT$.[18] The high value of χ_{AB} is due to the representation of 14 monomers per coarse-grain segment and consistent with experimental values $\chi_{PS\text{-}PDMS} \approx 0.18$ for PS-PDMS monomers and $\chi_{PS\text{-}PDMS}N \approx 25$ for a PS_{28}-*b*-$PDMS_{112}$ polymer chain composed of 140 monomers.[7]

RESULTS AND DISCUSSION

To examine the effect of the experimentally tunable spacing of posts on the ordering of DBCP domains on the substrate, we simulated the DBCP melt in the absence of posts (Figure 2), in the presence of posts arranged in hexagonal arrays of variable spacing (Figure 3), and in the presence of posts arranged in square arrays of variable spacing (Figure 4).

Absence of Posts. In the absence of posts, we observe the formation of a thin film of component A in contact with the substrate and of a hexagonal array of spherical domains of component A in the matrix of component B (Figure 2). The hexagonal morphology agrees with experimental observations,[7,8] and the average center-to-center distance between spherical domains of A in the neat block copolymer was identified to be $L_0 = 12.4 \pm 0.1$ lattice sites. Small deviations from ideal hexagonal geometry (Figure 2) are associated with a mismatch between the hexagonal domain order and

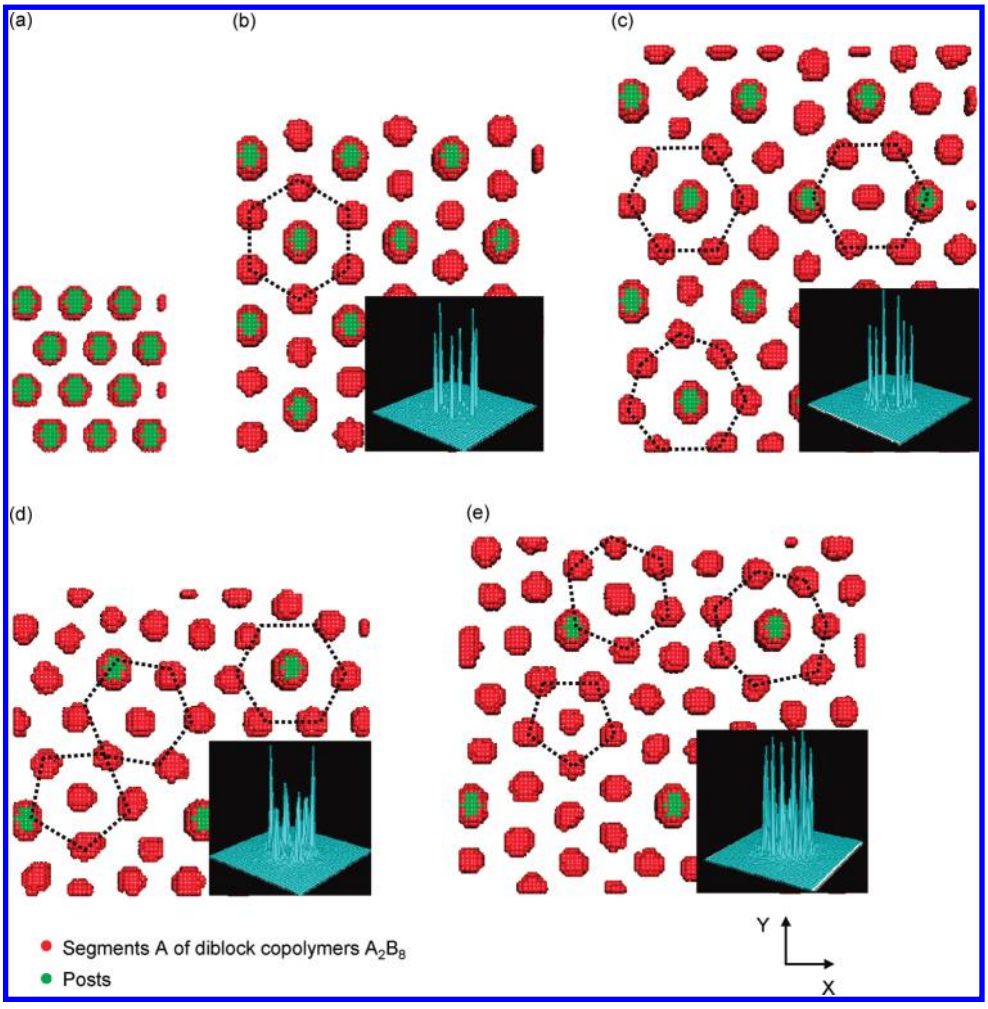

Figure 3. Computed average morphologies of spherical domains of A in a A_2B_8 diblock copolymer film between two parallel flat surfaces containing a hexagonal array of posts. The spacing between posts $L_{P,HEX}$ in units of L_0 varied in the order (a) 0.97, (b) 1.94, (c) 2.26, (d) 3.39, (e) 3.87. The formation of perfect hexagonal patterns (a, b) as well as patterns with perturbed long-range order (c−e) can be seen. Dashed lines indicate hexagonal, distorted hexagonal, pentagonal, and heptagonal features. The insets show Fourier transforms of the position of domains A and posts to aid in the evaluation of long-range order.

the quadratic boundaries of the periodic lattice in the *xy* plane (72 × 72 × 14 lattice sites). L_0 remained the same for four times the lattice area in the *xy* plane within ±0.1 units.

Hexagonal Arrays of Posts. In the presence of hexagonal arrays of posts on the substrate, simulation of the DBCP melt resulted in thin films of component A in contact with the substrate and with the posts, as well as patterns of spherical domains of component A in the matrix of component B (Figure 3). All patterns of domains A display perfect hexagonal structures with long-range order or symmetry-broken structures with hexagonal elements as well as pentagonal and heptagonal elements that prevent long-range order (Figure 3). The computed patterns can be directly compared to scanning electron microscopy (SEM) images of patterns of cylindrical PS domains in PS-PDMS block copolymers on a hydrogen silsesquioxane surface as a function of the ratio $L_{P,HEX}/L_0$.[7] The ratio between the surface area per post, $A_{P,\ HEX} = \sqrt{3}/2L^2_{P,\ HEX}$ (Figure 1b), and the surface area per domain of A in the neat block copolymer, $A_0 = \sqrt{3}/2L_0^2$ (Figure 1e), has major influence on the observed pattern and long-range symmetry:

$$N_{D,HEX} = \frac{A_{P,HEX}}{A_0} = \left(\frac{L_{P,HEX}}{L_0}\right)^2 \quad (1)$$

$N_{D,HEX}$ equals the preferred number of domains of A per post, including the covered post as a domain,[19] and imposes constraints on the packing of spherical domains of A.

For $L_{P,HEX}/L_0 = 0.97$ and $N_{D,HEX} = 0.94$,[20] a well-defined hexagonal pattern is seen in the simulation that contains one domain of component A per post covering its surface (Figure 3a). This pattern is identical to the pattern reported in experiment for $L_{P,\ HEX}/L_0 = 1.0$ and $N_{D,\ HEX} = 1.0$.[7] For a larger spacing $L_{P,HEX}/L_0 = 1.94$ and $N_{D,HEX} = 3.8$, we also observe a well-defined hexagonal pattern (Figure 3b). It involves three domains of component A per post, has been observed in

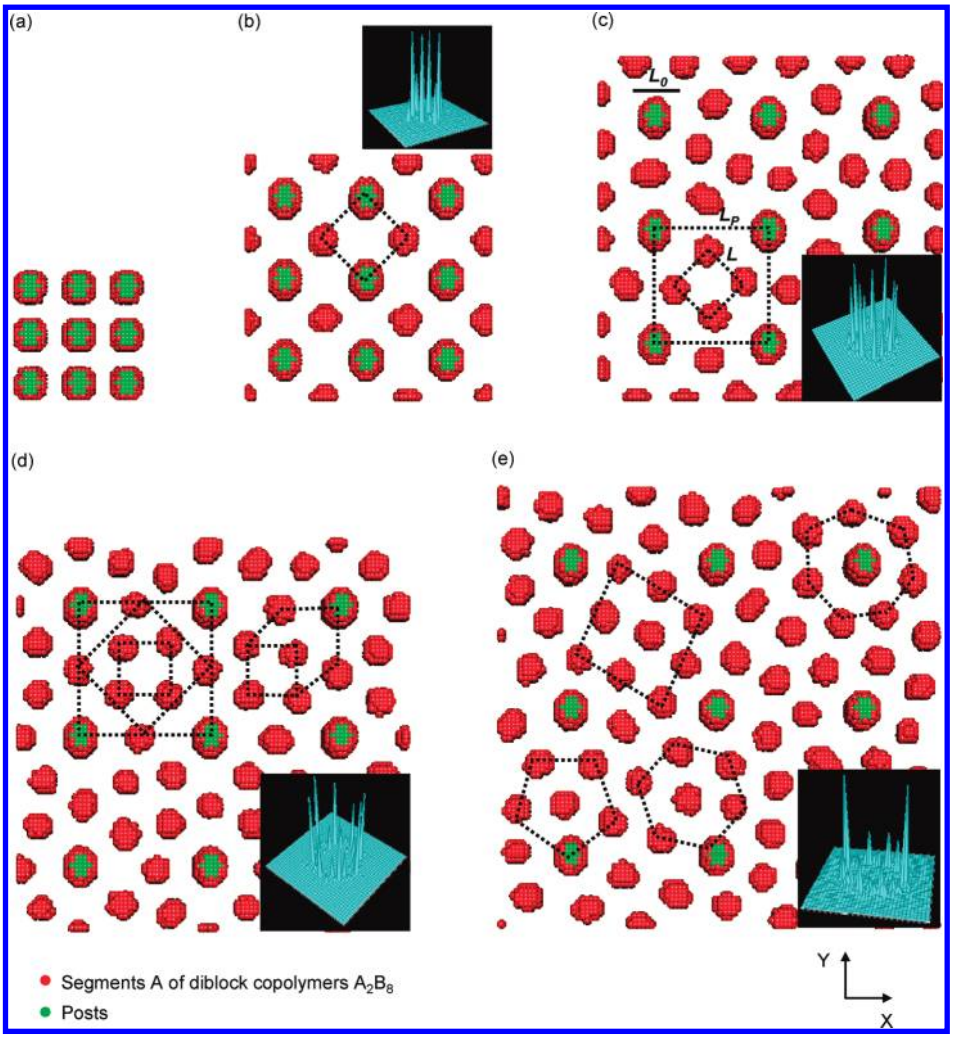

Figure 4. Computed average morphologies of spherical domains of A in A_2B_8 diblock copolymer films between two parallel flat surfaces containing square arrays of posts. The spacing between posts L_P in units of L_0 varied in the order (a) 0.97, (b) 1.61, (c) 1.94, (d) 2.58, and (e) 2.90. Dashed lines indicate square, nested square, and remotely ordered morphologies. The insets show Fourier transforms of the position of domains A and posts to aid in the evaluation of long-range order.

experiment,[7,21] and appears to be more stable than a pattern of four domains per post. For $L_{P,HEX}/L_0 = 2.26$ and $N_{D,HEX} = 5.1$, we observe a slightly disordered pattern that involves mostly four and sometimes five domains of component A per post (Figure 3c).[20] The structure is close to a perfect hexagonal pattern of four domains per post that was observed in experiment.[7] Since the preferred number of 5.1 domains per post exceeds the optimum value of four domains per post, small additional domains break the hexagonal symmetry (see highlighted heptagon in Figure 3c). For $L_{P,HEX}/L_0 = 3.39$ and $N_{D,HEX} = 11.5$, the pattern contains about 11 domains of component A per post and cannot achieve perfect hexagonal order, consistent with experiment (Figure 3d).[7] The structure consists of distorted pentagonal, hexagonal, and heptagonal elements. For $L_{P,HEX}/L_0 = 3.87$ and $N_{D,HEX} = 15$, we find a similar distorted hexagonal pattern containing 15 domains of component A per post (Figure 3e).

The experimental investigation of many ratios $L_{P,HEX}/L_0$[7] shows that, after conversion of $L_{P,HEX}/L_0$ to $N_{D,HEX}$ according to eq 1, the "magic numbers" $N_{D,HEX}$ that enable a perfect hexagonal pattern are 1, 3, 2^2, 7, and 3^2. When $N_{D,HEX}$ is larger, the numbers 13, 4^2, and 21 also yield locally stable hexagonal patterns, although multiple orientations of DBCP domains were found in the templates.[7] As $N_{D,HEX}$ assumes large values, long-range instability occurs because free energy differences between different orientations of DBCP domains become smaller. The findings by experiment and simulation suggest that the ratio of the surface area occupied per post in relation to the surface area occupied per spherical domain of component A, $N_{D,HEX}$, is important to control long-range order and needs to equal certain integer numbers to produce a pattern of hexagonal symmetry. The preferred numbers $N_{D,HEX}$ enabling perfect order must also be small enough, and already minor deviations can break the symmetry, especially for a larger number $N_{D,HEX}$.

TABLE 1. Comparison of the Spacing between Posts in a Square Array L_P, Preferred Number of Domains A per Post N_D, and Observed Number of Domains A per Post by Simulation[a]

spacing of posts L_P (in units of L_0)	preferred number of domains A per post N_D (eq 2)	number of domains A per post (sim)	Figure
0.97	1.1	1	4a
1.61	3.0	2	4b
1.94	4.3	5	4c
2.58	7.7	7	4d
2.90	9.7	9−10	4e

[a] Well-ordered structures are formed for certain integer values of N_D (1, 2, 5, 7).

Square Arrays of Posts. In the presence of square arrays of posts on the substrate, simulation of the DBCP melt resulted in thin films of component A in contact with the substrate and with the posts, as well as patterns of spherical domains of component A in the matrix of component B (Figure 4). Similar to the hexagonal array of posts, the pattern of component A correlates with the ratio between the surface area per post, $A_P = L_P^2$, and the equilibrium surface area per spherical domain A in the neat diblock copolymer, $A_0 = \sqrt{3}/2L_0^2$ (Figure 1c and e):

$$N_D = \frac{A_P}{A_0} = \frac{2\sqrt{3}}{3}\left(\frac{L_P}{L_0}\right)^2 \quad (2)$$

The pattern of component A contains preferably N_D domains of A per post, whereby the A-attracting posts contribute one domain of A (Table 1).[19] As a function of the spacing of posts L_P in units of L_0, only certain integer values of N_D facilitate a geometric arrangement with long-range order, and the patterns adjust to the nearest "magic number" by variation of domain size within a certain range (Figure 4 and Table 1). The definition of a pattern is the closer the spacing between posts L_P matches preferred values of N_D, the smaller the preferred values N_D. Pattern definition and long-range stability decrease for high numbers of N_D because the preference of the block copolymer domains toward local hexagonal coordination interferes with the prescribed square order of the templates (Figure 4e).

We examine these findings for a series of square spacing between posts L_P from 0.97 to 2.9 in units of L_0 (Figure 4 and Table 1).[21] The preferred number of domains per post N_D ranges from 1.1 to 9.7 in this series (eq 2). For a spacing of posts $L_P \leq 0.97L_0$ we expect ≤1.1 preferred domains of A per post (Table 1). In agreement, segments A adsorb on the attractive post surface and no neat domains of A are found in the matrix B (Figure 4a). This morphology reflects the similarity in surface areas per post A_P and per domainA_0.

An increased post spacing of $L_P = 1.61L_0$ leads to 3.0 preferred domains of A per post (Table 1). We find segments A adsorbed on the post surface and one additional domain of A in the center of each square unit (Figure 4b). The pattern corresponds to two domains of A per post, however, and the difference from the expectation value $N_D = 3$ is related to the geometric challenge to accommodate three units of A per post in a square pattern with long-range symmetry. Therefore, the system forms two domains per post in which the side length L of the square array of domains A increased to $1.14L_0$ relative to its equilibrium value $0.93L_0$. The density of domains A per unit surface area is twice the density of lithographic posts, which has not yet been reported in experimental systems.

An increased post spacing of $L_P = 1.94L_0$ leads to 4.3 preferred domains of A per post (Table 1). Domains of A then form nested squares inside the squares of posts (Figure 4c). The pattern corresponds to 5 domains of A per post, and each post is surrounded by 8 domains of A in octagonal coordination. The preference for 5 domains of A per post arises from the geometric challenge to accommodate a periodic pattern of 4 domains per post with equal nearest neighbor spacing. Since the area density of posts is somewhat higher compared to the ideal case $N_D = 5$ ($L_P = 2.08L_0$), domains of A are packed more densely and the degree of order may be lower than in the ideal structure. In comparison to denser prepatterns such as the square array at $L_P = 1.61L_0$ (Figure 4b), the degree of order appears more sensitive to the exact spacing.

A further increased spacing of posts of $L_P = 2.58L_0$ leads to 7.7 preferred domains of A per post (Table 1). We find a periodic pattern of two nested squares of domains A per unit square of posts, in which the vertex of smaller squares is located at the center of the edge of the next bigger square (Figure 4d). The observed structure corresponds to seven domains per post, and the difference from $N_D = 7.7$ slightly widens the structure, leading to some deviation from the ideal pattern. Nevertheless, all features remain closer to square and octagonal coordination than to hexagonal (highlights in Figure 4d). The observed morphology also indicates that eight domains of A per post, with an additional domain in the center of each square of posts, may not yield a stable geometry.

The largest spacing of posts $L_P = 2.90$ examined here leads to 9.7 preferred domains of A per post (Table 1). A long-range ordered structure of the DBCP domains cannot be identified, and instead a mixed structure with 9 to 10 domains of A per post is found (Figure 4e). The arrangement of domains of A is disordered with a major amount of hexagonal elements, as well as square, pentagonal, and heptagonal elements (highlights in Figure 4ee). A transition to a nonsquare morphology has occurred.

The observed trends in the morphology of DBCP domains A as a function of the spacing of posts are

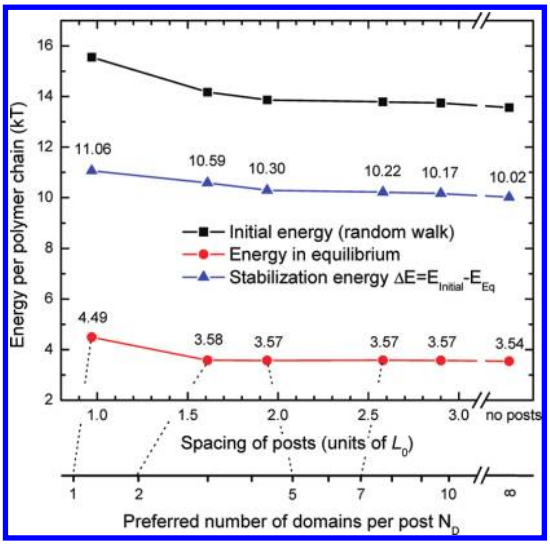

Figure 5. Average initial energy, equilibrium energy, and stabilization energy ΔE of diblock copolymers on a substrate containing a square array of posts as a function of the spacing of posts. The energy of the initial random structure and the stabilization energy decrease upon increased spacing of posts. A minimum is reached for the neat block copolymer (no posts). The equilibrium energy is much lower than the initial energy and remains nearly the same for larger spacing of posts. Dashed lines indicate the connection between the preferred and observed numbers of spherical domains per post.

associated with thermodynamic trends. To examine this relation, we computed average energies of initial random morphologies, average energies of the self-assembled equilibrium structures, and the difference between the two, which represents the stabilization energies ΔE upon assembly (Figure 5, see Methods section for computational details). From small spacing of posts toward wide spacing of posts, initial energies decrease from higher values to lower values, which is associated with a decrease in total interfacial contact area between the DBCP domains and the posts. The energy of equilibrium structures is significantly lower than the initial energy and hardly changes for spacing of posts greater than $1.5L_0$ (Figure 5). The stabilization energy ΔE is higher for a dense spacing than for a sparse spacing of posts. This trend reflects the high structural definition and possible long-range order for a dense spacing of posts (Figure 4ea,b) in comparison to decreasing pattern definition and long-range order for a wider spacing of posts (Figure 4c,d,e). In the absence of posts, the stabilization energy reaches a minimum, equivalent to no template effect (Figure 2b). Differences in stabilization energies between model PS-PDMS morphologies for increasing spacing of posts, as shown in Figure 4e, are on the order of 0.10 kT per block copolymer chain, or 0.06 kcal per mol of block polymer chain (Figure 5). Associated changes in stabilization entropies remained difficult to compute reliably. As an estimate, we believe that the local mobility of chains does not differ greatly from one pattern to another, so that differences in entropy among various equilibrium morphologies are also small.

In summary, square order and significant structural stability for low values of N_D close to "magic numbers" are associated with higher stabilization energies in comparison to the neat DBCP (Figure 5).

Influence of Other Parameters. In addition to suitable ratios of the surface area per post and per block copolymer domain, the template structures contain other features that affect the pattern of spherical or cylindrical DBCP domains. These include the composition of the block copolymer, the length of the blocks, the film thickness, the composition, and geometry of the posts. Some parameters can be varied, and others are predetermined by the aim to generate homogeneous, well-ordered structures.

Major variables are the chemical nature and length of the polymer blocks. A larger interfacial energy between the two blocks supports the formation of patterns with long-range order due to enhanced phase separation. The relative length of the blocks determines whether sphere or cylinder morphologies of component A are formed. The choice of PS-PDMS block copolymers in this work is typical,[7,8] and interface energies could be enhanced or weakened by choice of different monomers. The principle of preferred numbers of domains per area remains the same when interfacial energies change. The concept of preferred integer numbers N_D also applies whether sphere or cylinder morphologies are present because cylinders form the same native hexagonal pattern as spheres and extend normal to the surface plane.[22] Consistency between experiments on hexagonal patterns of cylinders[7] and simulation of hexagonal patterns of spheres was shown (see subsection on hexagonal arrays of posts).

The geometry of the film and of the posts is largely predetermined. The thickness of the DBCP film H determines the number of layers of spherical DBCP domains. Control over layer thickness is thus of importance and can be, for example, optimized to support one layer of spherical domains. The impact of layer thickness can be reduced when the block copolymers are designed to form cylindrical domains instead of spheres. To maximize confinement and long-range order, the height of the posts H_P must be close to the film thickness H. Shorter posts reduce graphoepitaxy and worsen the definition of patterns. Further, a similar thickness of posts and DBCP domains is favorable to obtain homogeneous ordered structures. Therefore, the thickness of the posts is essentially predetermined, and we anticipate that minor changes in thickness have little impact on the assembly of DBCP domains since the volume fraction of posts is small.

The composition of the surface of the posts is also largely predetermined. To act as an effective template, the post surface should attract the minor component

of the DBCP. If the post surface prefers contact with the major component of the DBCP, the posts would integrate into the matrix of the major component without a significant template effect toward hexagonal or square order of the minor component, especially at the desired low area density of posts.[19]

We emphasize that all foregoing parameters are important to optimize details of self-assembled structures and long-range order. The systematic analysis of their impact, however, exceeds the scope of this work and remains a future task. In this contribution, we have clarified the role of the arguably most important parameter, the spacing between posts, to control the type of pattern derived.

CONCLUSIONS

We analyzed equilibrium patterns of spherical domains of thin diblock copolymer films deposited on substrates containing hexagonal and square arrays of posts of variable spacing. We employed Monte Carlo simulation for systems similar to PS-PDMS diblock copolymers. A major parameter controlling the formation of ordered *versus* irregular patterns of the minor component (PS) is the ratio between the surface area per post and the surface area per neat block copolymer domain N_D (eqs 1 and 2), which can be adjusted by the spacing of posts in relation to the equilibrium spacing of the block copolymer domains L_P/L_0. N_D corresponds to the preferred number of DBCP domains per post, and certain integer numbers lead to well-ordered structures. For hexagonal patterns of posts, these numbers are 1, 3, 4, 7, and 9 according to previous experiments[7] and simulation, and all such domain patterns are hexagonal. For square patterns of posts, preferred numbers N_D are 1, 2, 5, and 7 domains per post according to simulation, and they lead to well-ordered structures with square and nested square geometries. Higher numbers reduce the effectiveness of the square template by introduction of hexagonal elements into the structure, and also nonideal numbers N_D facilitate disorder. Disordered morphologies are characterized by the simultaneous occurrence of multiple structural elements such as square, pentagonal, hexagonal, heptagonal, and octagonal geometries. The area density of square DBCP domains can be increased up to 7-fold in nested structures compared to the square template. Such square patterns on the sub-50 nm scale, which have not yet been obtained experimentally, provide a pathway to produce circuit boards with more than 10^{11} computing and storage units per cm^2. Monte Carlo simulation using verified models is helpful to analyze equilibrium morphologies and stabilization energies, and further details of the influence of the composition of the block copolymer and of geometric parameters of the templates remain to be explored in future work.

METHODS

Models. In the models, two confining surfaces (S), posts (P), DBCP chains of composition A_2B_8, and vacancies (V) were represented by coarse-grain beads on a cubic lattice of variable size (Figure 1). The surfaces correspond to the outside of the lattice, and the size of the cubic lattice varied from system to system from 36 × 36 × 14 up to 144 × 144 × 14 lattice sites. Each post occupied 17 lattice sites in the *xy* plane and had a height of 10 lattice sites (Figure 1b,c). In the remaining space, the volume fraction of the polymer was 0.833 and the volume fraction of vacancies 0.167. The beads of coarse-grain DBCP chains were connected through permissible bond lengths of 1 and $(2)^{1/2}$ lattice units. For each system, initial models of ordered block copolymers and vacancies were generated. The size of the lattice was $L_x \times L_y \times 14$, and the number of polymer chains N varied as follows. For the system without posts (Figure 2), we chose $L_x = L_y = 72$ and $N = 6048$ as well as $L_x = L_y = 144$ and $N = 24\,192$. For the systems containing a hexagonal array of posts (Figure 3), we chose (a) $L_x = 36$, $L_y = 42$, and $N = 1560$, (b) $L_x = 72$, $L_y = 80$, and $N = 6516$, (c) $L_x = 84$, $L_y = 96$, and $N = 9204$, (d) $L_x = 84$, $L_y = 72$, and $N = 6988$, (e) $L_x = 96$, $L_y = 84$, and $N = 9340$. For the systems containing a square array of posts (Figure 4), we chose (a) $L_x = L_y = 36$ and $N = 1359$, (b) $L_x = L_y = 60$ and $N = 4047$, (c) $L_x = L_y = 84$ and $N = 8079$, (d) $L_x = L_y = 96$ and $N = 10\,599$, (e) $L_x = L_y = 108$ and $N = 13\,455$.

Interaction Potential. The total potential energy was obtained by pairwise summation of the interaction energies between all nearest nonbonded neighbor segments. The interaction energy included a repulsion of $0.5kT$ between nonbonded segments A and B, between the surface and component B, and between the posts and component B. All other pairwise interaction energies were zero (see introduction).

Computation. We employed a Monte Carlo algorithm with stochastic motions of vacancy diffusion[23] and bond fluctuation[24] until thermodynamic equilibration was reached. Displacements of the vacancies led to faster equilibration of the dense polymer melt than displacements of the polymer beads.[14,16,25] Displacements of vacancies and adjustments of the polymer structure were limited by excluded volume, allowed bond lengths of 1 and $(2)^{1/2}$, and exclusion of bond-crossing moves. The Metropolis criterion was invoked to evaluate the acceptability of each attempted move.[26−28]

For every system, we carried out three separate simulations with different pre-equilibrated configurations and observed convergence to one consistent average final morphology. Every simulation was divided into two parts: (1) In the first part, start structures were subjected to random self-avoiding walks with interaction potentials of zero between all nonbonded components (S, P, A, B, V) for 2.5 million Monte Carlo steps times the number of vacancies. The corresponding average energy, normalized per polymer chain, is shown as initial energy in Figure 5. (2) In the second part, the pre-equilibrated structures were subjected to simulation with the full interaction potential for 10 million Monte Carlo steps times the number of vacancies. The average acceptance rate of Monte Carlo motions was 0.22, far from equilibrium, and decreased to 0.09 toward equilibrium for all simulations. The average energy is shown as equilibrium energy in Figure 5.

Analysis. The analysis involved visual inspection of the morphologies, particularly the pattern of spherical domains of component A, and monitoring of the convergence of the total energy. In the top view in Figures 2, 3, and 4, lattice positions between 4 and 9 in the *z* direction are shown. The morphologies represent the average occupancy $\phi(r)$ of lattice sites r with

spherical domains of component A, using the instantaneous occupancy $\rho(r,i)$ as an average over $n = 100$ sample snapshots i in equilibrium, distributed over the last 1 million Monte Carlo steps:

$$\phi(r) = \frac{1}{n}\sum_{i=1}^{n} \rho(r,i) \quad (3)$$

Hereby, the occupancy of lattice site r in a single snapshot i is $\rho(r,i) = 1$ when occupied by segment A, $\rho(r,i) = 0$ when occupied by a vacancy, and $\rho(r,i) = -1$ when occupied by segment B. The average occupancy $\phi(r)$ of a lattice site r over all snapshots, as shown in Figures 2, 3, and 4, was attributed to segments A when $\phi(r) > 0$ (red), to vacancies when $\phi(r) = 0$, and to segments B when $\phi(r) < 0$ (white background).

The average patterns of DBCP domains A were processed into scattering patterns $S(q)$ by Fourier transformation, as shown in the insets of Figures 2, 3, and 4:

$$\psi_q = \int_0^{L_x} \mathrm{d}x \int_0^{L_y} \psi(x,y)\exp[i(q_x x + q_y y)]\,\mathrm{d}y \quad (4)$$

$$S(q) = \frac{\psi_{-q}\psi_q}{L^3} \quad (5)$$

Hereby, $\psi(x,y)$ is an order parameter equal to 1 when the position (x,y) was occupied by segment A or by the post surface; otherwise, $\psi(x,y) = 0$. The scattering vector q was given as $q = (q_x,q_y) = 2\pi(m_x/L_x,m_y/L_y)$ with integer numbers m_x, m_y, and the length of the lattice L_x, L_y in x, y directions. An intense peak at the origin of the scattering pattern is not shown for clarity.

Acknowledgment. We are grateful for support by the National Science Foundation (DMR-0955071), the Air Force Research Laboratory, the Ohio Department of Development, and the University of Akron. We are thankful to the Ohio Supercomputing Center for the allocation of computational resources.

REFERENCES AND NOTES

1. Del Campo, A.; Arzt, E. Fabrication Approaches for Generating Complex Micro- and Nanopatterns on Polymeric Surfaces. *Chem. Rev.* **2008**, *108*, 911–945.
2. Black, C. T.; Guarini, K. W.; Milkove, K. R.; Baker, S. M.; Russell, T. P.; Tuominen, M. T. Integration of Self-Assembled Diblock Copolymers for Semiconductor Capacitor Fabrication. *Appl. Phys. Lett.* **2001**, *79*, 409–411.
3. Tang, C. B.; Lennon, E. M.; Fredrickson, G. H.; Kramer, E. J.; Hawker, C. J. Evolution of Block Copolymer Lithography to Highly Ordered Square Arrays. *Science* **2008**, *322*, 429–432.
4. Park, S.; Lee, D. H.; Xu, J.; Kim, B.; Hong, S. W.; Jeong, U.; Xu, T.; Russell, T. P. Macroscopic 10-Terabit−per−Square-Inch Arrays from Block Copolymers with Lateral Order. *Science* **2009**, *323*, 1030–1033.
5. Bates, F. S.; Fredrickson, G. H. Block Copolymer Thermodynamics: Theory and Experiment. *Annu. Rev. Phys. Chem.* **1990**, *41*, 525–557.
6. Darling, S. B. Directing the Self-Assembly of Block Copolymers. *Prog. Polym. Sci.* **2007**, *32*, 1152–1204.
7. Bita, I.; Yang, J. K. W.; Jung, Y. S.; Ross, C. A.; Thomas, E. L.; Berggren, K. K. Graphoepitaxy of Self-Assembled Block Copolymers on Two-Dimensional Periodic Patterned Templates. *Science* **2008**, *321*, 939–943.
8. Ruiz, R.; Kang, H. M.; Detcheverry, F. A.; Dobisz, E.; Kercher, D. S.; Albrecht, T. R.; de Pablo, J. J.; Nealey, P. F. Density Multiplication and Improved Lithography by Directed Block Copolymer Assembly. *Science* **2008**, *321*, 936–939.
9. Jung, Y. S.; Ross, C. A. Well-Ordered Thin-Film Nanopore Arrays Formed Using a Block-Copolymer Template. *Small* **2009**, *5*, 1654–1659.
10. Stoykovich, M. P.; Kang, H. M.; Daoulas, K. C.; Liu, G. L.; Liu, C. C.; de Pablo, J. J.; Mueller, M.; Nealey, P. F. Directed Self-Assembly of Block Copolymers for Nanolithography: Fabrication of Isolated Features and Essential Integrated Circuit Geometries. *ACS Nano* **2007**, *1*, 168–175.
11. Park, S. M.; Craig, G. S. W.; La, Y. H.; Solak, H. H.; Nealey, P. F. Square Arrays of Vertical Cylinders of PS-*b*-PMMA on Chemically Nanopatterned Surfaces. *Macromolecules* **2007**, *40*, 5084–5094.
12. Yang, X. M.; Wan, L.; Xiao, S. G.; Xu, Y. A.; Weller, D. K. Directed Block Copolymer Assembly *versus* Electron Beam Lithography for Bit-Patterned Media with Areal Density of 1 Terabit/inch^2 and Beyond. *ACS Nano* **2009**, *3*, 1844–1858.
13. Wang, Q.; Yan, Q. L.; Nealey, P. F.; de Pablo, J. J. Monte Carlo Simulations of Diblock Copolymer Thin Films Confined between Two Homogeneous Surfaces. *J. Chem. Phys.* **2000**, *112*, 450–464.
14. Feng, J.; Ruckenstein, E. The Morphology of Symmetric Triblock Copolymer Melts Confined in a Slit: A Monte Carlo Simulation. *Macromol. Theory Simul.* **2002**, *11*, 630–639.
15. Yu, B.; Sun, P. C.; Chen, T. H.; Jin, Q. H.; Ding, D. T.; Li, B. H.; Shi, A. C. Confinement-Induced Novel Morphologies of Block Copolymers. *Phys. Rev. Lett.* **2006**, *96*, 138306.
16. Feng, J.; Ruckenstein, E. Morphologies of AB Diblock Copolymer Melts Confined in Nanocylindrical Tubes. *Macromolecules* **2006**, *39*, 4899–4906.
17. Pandey, R. B.; Heinz, H.; Feng, J.; Farmer, B. L.; Slocik, J. M.; Drummy, L. F.; Naik, R. R. Adsorption of Peptides (A3, Flg, Pd2, Pd4) on Gold and Palladium Surfaces by a Coarse-Grained Monte Carlo Simulation. *Phys. Chem. Chem. Phys.* **2009**, *11*, 1989–2001.
18. Freire, J. J.; McBride, C. Mesophase Formation in Solutions of Diblock Copolymers Simulated Using the Bond Fluctuation Model. *Macromol. Theory Simul.* **2003**, *12*, 237–242.
19. The preferred number of domains of neat component A per post is $N_{D,HEX} - 1$ and $N_D - 1$, plus the post covered by component A, which yields a total of $N_{D,HEX}$ and N_D, respectively, domains of component A per post. If the posts repel component A, all domains of A would be embedded in the matrix of component B. Then, the preferred number of domains A per post equals $N_{D,HEX}$ and N_D. However, without coverage of the posts by domains A, the template effect of the posts would be diminished.
20. Fractional numbers result from the discrete lattice size.
21. In ref 7, three spherical domains of the minor DBCP component per post were observed for $L_{P,\ HEX} = 1.65L_0$, $N_{D,\ HEX} = 2.7$. Two domains were found inside each parallelogram of posts and one on the post surface, exactly as in the simulation.
22. The choice of spheres was more convenient in this computational study. Cylinder morphologies in the model require a larger box height and a higher number of Monte Carlo steps for equilibration, which was challenging to complete for a wide range of template spacing.
23. Reiter, J.; Edling, T.; Pakula, T. Monte Carlo Simulation of Lattice Models for Macromolecules at High Densities. *J. Chem. Phys.* **1990**, *93*, 837–844.
24. Larson, R. G.; Scriven, L. E.; Davis, H. T. Monte Carlo Simulation of Model Amphiphile-Oil−Water Systems. *J. Chem. Phys.* **1985**, *83*, 2411–2420.
25. Pandey, R. B.; Anderson, K. L.; Heinz, H.; Farmer, B. L. Conformation and Dynamics of a Self-Avoiding Sheet: Bond-Fluctuation Computer Simulation. *J. Polym. Sci., Part B* **2005**, *43*, 1041–1046.
26. Metropolis, N.; Rosenbluth, A. W.; Rosenbluth, M. N.; Teller, A. H.; Teller, E. Equation of State Calculations by Fast Computing Machines. *J. Chem. Phys.* **1953**, *21*, 1087–1092.
27. Frenkel, D.; Smit, B. *Understanding Molecular Simulation: From Algorithms to Applications*; Academic Press: San Diego, 2002.
28. Pandey, R. B.; Heinz, H.; Feng, J.; Farmer, B. L. Biofunctionalization and Immobilization of a Membrane via Peptide Binding (CR3-1, S2) by a Monte Carlo Simulation. *J. Chem. Phys.* **2010**, *133*, 095102.